

## Article

# The Impact of Clogging Issues at a Riverbank Filtration Site in the Lalin River, NE, China: A Laboratory Column Study

Bin Hu <sup>1,2,3</sup>, Linmei Liu <sup>4</sup>, Ruihui Chen <sup>5</sup>, Yi Li <sup>6</sup>, Panwen Li <sup>7</sup>, Haiyang Chen <sup>4</sup>, Gang Liu <sup>1,2,\*</sup> and Yanguo Teng <sup>4,\*</sup>

<sup>1</sup> Stake Key Laboratory of Environmental Aquatic Chemistry, Research Center for Eco-Environmental Science, Chinese Academy of Sciences, Beijing 100085, China; binhu@rcees.ac.cn

<sup>2</sup> University of Chinese Academy of Sciences, Beijing 100049, China

<sup>3</sup> Engineering Research Center of Groundwater Pollution Control and Remediation, Ministry of Education, Beijing Normal University, Beijing 100875, China

<sup>4</sup> College of Water Sciences, Beijing Normal University, Beijing 100875, China; 202021470017@mail.bnu.edu.cn (L.L.); chen.haiyang@bnu.edu.cn (H.C.)

<sup>5</sup> Key Laboratory of Nonpoint Source Pollution Control, Ministry of Agriculture and Rural Affairs, Institute of Agricultural Resources and Regional Planning, Chinese Academy of Agricultural Sciences, Beijing 100081, China; chenruihui@caas.cn

<sup>6</sup> School of Civil Engineering, Architecture and Environment, Hubei University of Technology, Wuhan 430068, China; liyi\_bnuphd@mail.bnu.edu.cn

<sup>7</sup> Foreign Environmental Cooperation Center, Ministry of Ecology and Environment of China, Beijing 100035, China; li.panwen@fecomee.org.cn

\* Correspondence: gliu@rcees.ac.cn (G.L.); ygteng@bnu.edu.cn (Y.T.); Tel.: +86-10-6284-3096 (G.L.); +86-10-5880-2796 (Y.T.)



**Citation:** Hu, B.; Liu, L.; Chen, R.; Li, Y.; Li, P.; Chen, H.; Liu, G.; Teng, Y. The Impact of Clogging Issues at a Riverbank Filtration Site in the Lalin River, NE, China: A Laboratory Column Study. *Sustainability* **2022**, *14*, 9330. <https://doi.org/10.3390/su14159330>

Academic Editor: Beniamino Russo

Received: 26 June 2022

Accepted: 28 July 2022

Published: 29 July 2022

**Publisher's Note:** MDPI stays neutral with regard to jurisdictional claims in published maps and institutional affiliations.



**Copyright:** © 2022 by the authors. Licensee MDPI, Basel, Switzerland. This article is an open access article distributed under the terms and conditions of the Creative Commons Attribution (CC BY) license (<https://creativecommons.org/licenses/by/4.0/>).

**Abstract:** Although riverbank filtration (RBF) has been widely applied in China, the managers do not pay enough attention to the inevitable clogging issues during continuous RBF operation. The RBF site, which is located near the Lalin River, northeastern China, was selected as the study area, and the laboratory column experiments were used to simulate the RBF process and further investigate the physical and chemical clogging. The removal of turbidity (59.4–95.1%), COD (21.9–71.7%),  $\text{NH}_4^+$  (10.9–39.4%), Fe (18.5–64.8%), and Mn (19.8–71.7%) demonstrated the water quality improvement by RBF. Whereas, the significant decrease in permeability (39.6–88.2%) also indicated that the clogging issues could not be ignored during RBF. Among them, the physical clogging-dominated area, chemical clogging-dominated area, and the transition zone were located at 0–12.5%, 37.5–100%, and 12.5–37.5% of the infiltration pathway, respectively. Moreover, the concentration of suspended particle materials, mean size of riverbed sediments, and aquifer media are the major impact factors for physical clogging; the precipitation of soluble constituents and redox reaction and other hydrochemical processes were the major impact factors for chemical clogging. The conclusion of this study can contribute to managers alleviating the clogging issues and improving the effectiveness of the sustainable operation in the local RBF system.

**Keywords:** riverbank filtration; physical clogging; chemical clogging; column experiment; hydraulic conductivity

## 1. Introduction

Riverbank filtration (RBF) is a common approach for drinking water supply by motivating surface water infiltrating to subsurface flow during extraction, which can improve water quality and guarantee a sustainable quantity of water supply [1–3]. During the percolation processes, RBF can improve the groundwater quality after removing pollutants from the infiltrated river water [4]. According to the previous studies, RBF can effectively remove suspended solids, inorganic pollutants (e.g.,  $\text{NO}_3^-$ ,  $\text{NH}_4^+$ ) [5], heavy metals (e.g.,  $\text{Fe}^{3+}$ ,  $\text{Mn}^{2+}$ ) [6,7] organic trace pollutants (bentazone, carbamazepine, sulfadimidine, etc.) [8], and organic micropollutants (phenazone, simazine, iopromide,

etc.) [9], as well as pathogens and viruses (*Escherichia coli*, *Cryptosporidium*, *Giardia*, etc.) [10] within a certain residence time, which varies from days to months, and even up to years [11]. During the RBF, the physical, chemical, and microbiological processes, such as filtration, sorption, dilution, redox reaction, precipitation, biodegradation, etc., proceed along the pathway “river-riverbed sediments-aquifer” [12–14]. According to the experience in Germany and the Netherlands, after the residence time of 60 days, the quality of infiltrated water and groundwater can be significantly improved in the RBF sites [1,3]. Therefore, RBF is regarded as an efficient water treatment or pretreatment technique that is based on natural processes, and is widely used in many countries, including the USA, India, Germany, the Netherlands, and China [3,15–18].

Like other filters, to some degree, clogging issues in the infiltration areas are inevitable during the continuous operation of RBF [19]. The clogging can affect the permeability of the streambed and aquifer media, and further change the hydrodynamic conditions in the hyporheic zone and infiltration areas [20,21]. The clogging may not only occur on the surface of streambed med (external clogging), but also within porous media (internal clogging) [22–24]. Among them, external clogging is caused by the deposition of suspended solids, whereas internal clogging is due to the intrusion of smaller particles or dissolved solids in the pores of the porous media. During RBF, the mechanical sorption, chemical reaction (e.g., redox reaction, ion exchange), and microbial process (e.g., microbial activity, degradation, biofilm growth) can increase the grain size or the specific surface areas of the particles, resulting in the decrease of pore and decline of hydraulic conductivities [25–28]. Thus, the clogging types can also be classified into four types, which is according to their formation properties: (1) mechanical (e.g., gas entrapment); (2) physical (e.g., deposition and adsorption); (3) chemical (e.g., ion-exchange sorption); and (4) biological (e.g., bacterial, extracellular polymeric substance (EPS) and biofilm growth) [29–32].

The hydrodynamic conditions in the hyporheic zone and infiltration areas will be changed, such as the decline of RW infiltration rate and permeability in the hyporheic zone. Numbers of studies have investigated the impacts of clogging on RBF system operation, clogging mechanisms, and hydrological responses. For example, Hubbs (2006) found that the decrease in specific capacity of RBF wells can be 50–75% due to the riverbed clogging during the first three to five years of groundwater withdrawal [33]. Engesgaard et al. (2006) investigated biotic clogging with column experiments and revealed that the bioclogging can decrease relative bulk hydraulic conductivity by about 100 times in 30 days [34]. Westrich et al. (2007) also conducted column experiments to investigate biotic clogging, and found that hydraulic conductivity decreases 7.5 times after 15 days [35]. According to the in-situ experiments with the mobile experimental apparatus, Pholkern et al. (2015) demonstrated that the effect of external clogging is 7.7–31.1% and the effect of internal clogging is 60.7–92.3% in the RBF sites along the Ping River, Chiang Mai, Thailand [36]. Poojitha et al. (2021) used two different types of Ganges riverbed sediment to explore the effects of clogging on RBF, and the results demonstrated the declines of hydraulic conductivities and porosity of the filter materials were 47.2–93.4% and 48–81%, respectively [21]. As mentioned by Goldschneider et al. (2007), the existence of clogging is a debated issue [29]. On the one hand, clogging can increase the efficiency of water quality improvement during RBF due to its similar characteristics to the “Schmutzdecke” in engineered slow-sand filtration systems (rich in organic matter and high concentration of microorganisms) [19,37,38]. On the other hand, it can severely reduce the quantity of groundwater withdrawal in RBF systems, which further affects the sustainability of the drinking water supply [39,40]. Thus, the impacts of clogging on the riverbed at RBF sites are worth continuously studying on both the field-scale and laboratory-scale.

For China, the first RBF facility was in the northeast region in the 1930s; besides, there are more than 50 riverside source fields constructed along the Yellow River, and 15 RBF sites in Hai River and Luan River basins [3]. However, the clogging issues are rarely studied in China; Hu et al. (2016) reviewed the clogging types and relevant alleviating mitigating approaches [41]. Cui et al. (2021) revealed the effect of riverbed sediment flushing and

clogging on river-water infiltration rate, within in situ monitoring and numerical modeling in the Second Songhua River, Northeast China [27]. Although there are more than 300 RBF sites in China for sustainable drinking water supply, the sustainability of groundwater withdrawal and the improvement of water quality are still the major problems to be concerned [42–44]. Compared with the developed countries with wide applications of RBF (e.g., Germany, the Netherlands, USA, etc.), the numbers of studies on clogging in RBF sites are still not enough, and need further systematic study.

Thus, in this paper, we conducted laboratory-scale column studies to investigate the impact and characteristics of physical and chemical clogging issues at the RBF site with a long-distance infiltration pathway to the Lalin River, NE, China. Within the column experiments simulating the infiltration process in different infiltration distances, the aims of this study were to (1) estimate the effects of clogging influencing the hydraulic conductivity of the porous medium; (2) investigate the clogging mechanisms at the RBF system adjoining Lalin River, and (3) identify the principal influence factors that control the physical and chemical clogging processes.

## 2. Materials and Methods

### 2.1. Raw Water

Raw water used for laboratory-scale column experiments in this study was collected from the Lalin River, which was one of the major source waters for the drinking water treatment plants in Wuchang City, Heilongjiang Province, China. More than 1000 L of raw water was collected and stored in the custom tank for experiment use. The initial water quality of raw water was investigated, including suspended particles (turbidity), Fe,  $\text{NO}_3^-$ ,  $\text{NH}_4^+$ , Mn, etc., which were consistent with the water quality parameters analysis of outflow during the experiment, to estimate the improvement of water quality by RBF through simulated column experiment.

### 2.2. Experiment Set-Up

The Quaternary sediments were the dominant mediums in the aquifers, which were composed of fine sand, sandstone, and medium-coarse sandstone [45]. The porosity of the aquifer media was about 0.38; clay proportion and silt proportion were 6.5% and 2.3%, respectively [46]. Considering the characteristics of the aquifer media, the quartz sands with the grain size of 0.3–0.5 mm ( $d_{50} = 0.31$  mm) were used in the experiment. The grain sizes were selected in order to simulate the characteristics of the Quaternary aquifer in the RBF site near the Lalin River. The experimental set-up consisted of 4 transparent plexiglass columns ( $L = 200$  mm,  $D = 45$  mm) in series, which were filled with the quartz sands mentioned above (Figure 1). To avoid layering, the columns were tapped in every increment of 4 cm during filling. To prevent leaching of the fillers, the columns were fitted with caps that contained filter cloth (50  $\mu\text{m}$ ) at the bottom and top of the columns. To avoid air entrapment, the inflow (Lalin River water) was pumped from the bottom in the first column (Figure 1). The experiment was conducted at 12–15 °C to simulate the environmental temperature of the local aquifer.

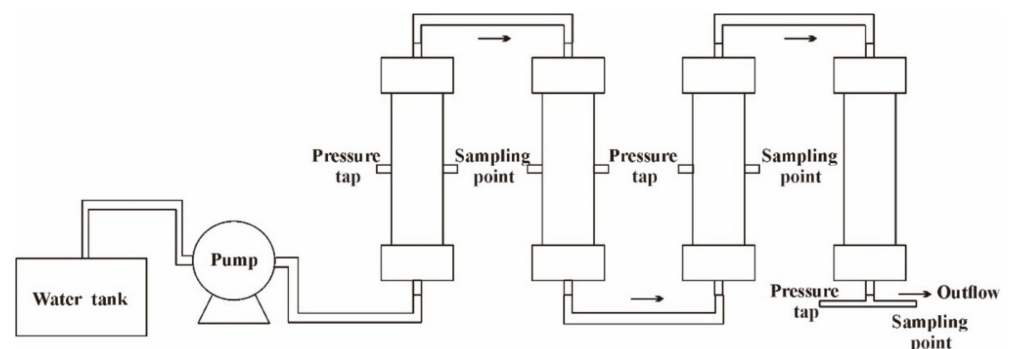


**Figure 1.** The structure of the column in the experiment.

Before the experiment, the  $\text{HgCl}_2$  was applied to the biocidal treatment of the filled quartz sands in the columns. The system was rinsed with DI water for 24 h by peristaltic pumps.

### 2.3. Operational Conditions of the Column Experiments

During the experiment phase, the infiltrated water was the raw water, which is mentioned in Section 2.1, and pumped into the columns through pumps with the rates of  $5.4 \text{ L h}^{-1}$  (0–144 h) and  $8.1 \text{ L h}^{-1}$  (144–216 h), respectively. Considering the ratio between the simulated infiltration pathway (80 cm) and the real infiltration pathway (3000 m), the pumping rate of  $5.4 \text{ L h}^{-1}$  was similar to the practical single wells exploitation after scaling down at the same proportion. Meanwhile, 1.5 times the pumping rate was used to evaluate the variation of clogging during the water peak period.

Totally, there were 4 sampling sites in the system, within the different infiltration distances (from the bottom of the first column to the bottom of the last column) of 10 cm, 30 cm, 50 cm, and 80 cm, respectively. To lower the impact of water sample collection on hydraulic retention time (HRT) as much as possible, a continual sample collection process was applied, during which the reactors were operated under normal conditions, and the corresponding sampling port was opened as the only effluent of the whole setup. To avoid influencing the HRT of other samples, during each sampling, the sample at 80 cm was first to be collected and the sample at 10 cm was the last.

Simultaneously, the discharge at the outlet of the permeameter was determined using a measuring flask and stopwatch. With the known difference in head between the first and last piezometers, the hydraulic gradient is calculated, and then by using Darcy's equation, permeability is computed at subsequent time intervals.

### 2.4. Water Quality Parameters

The sampling sites and hydraulic head monitoring (digital decline pressure sensor, CY201) were located at infiltration distances of 10 cm, 30 cm, 50 cm, and 80 cm, respectively. The water sampling for measurement was once per 24 h, and the hydraulic head was once per minute. Each water sample was divided into two parts: one was used to measure turbidity with spectrophotometry (national determination of turbidity, GB13200-1991), and the other one was used to analyze other water quality parameters after being filtered with  $0.45 \mu\text{m}$  glass fiber filters, which reproducibly removed particulates but passed the dissolved chemicals into the filtrate. The other water quality parameters, including COD,  $\text{NO}_3^-$ ,  $\text{NH}_4^+$ ,  $\text{Mn}^{2+}$ , total Fe,  $\text{Fe}^{2+}$ , etc., were analyzed with the potassium permanganate method, spectrophotometry (Shimadzu UV1780, Shimadzu Corporation, Kyoto, Japan), and a plasma spectrometer (ICP-MS, Agilent 7500C, Agilent Technologies Inc., Santa Clara, CA, USA), respectively.

### 2.5. Data Analysis

The statistical software package IBM SPSS Statistics for Windows version 20.0 was used to perform spearman correlation analysis and PCA (Supplementary Materials Tables S3 and S4). Network analysis was performed by Gephi 0.9.5 to estimate the impacts of physical and chemical clogging on RBF. There were 10 nodes and 45 edges in the network analysis. The permeability in the network analysis represented the decreased degree of relative hydraulic conductivity.

## 3. Results

### 3.1. Variation of Hydraulic Conductivities

The variation in hydraulic conductivity of the medium showed a continuous decrease trend and reached a steady state within 144 h (Figure 2). As shown in the Table S1, the relative hydraulic conductivities (RHC), represented by  $K/K_0$  ( $K$  was the real-time monitoring data,  $K_0$  was the initial hydraulic conductivity of the medium), ranged from 11.8% to 60.4% in the simulated RBF system (Table S1). The declines of RHC were increased with the

infiltration distance, which were 39.6–66.7% (average 60.4%), 48.7–78.3% (average 69.0%), 56.4–85.8% (average 76.6%), and 63.0–88.2% (average 80.1%) for the infiltration distance of 10 cm, 30 cm, 50 cm, and 80 cm, respectively (Table S2). In general, the RHC values of the mediums with different infiltration distances decreased sharply in the first 24 h, then the slope of the decrease became gentle with the increase of time, and finally reached a steady state at 144 h. It demonstrated that the permeability of the medium could keep declining and reach a steady state due to the clogging during RBF operation.

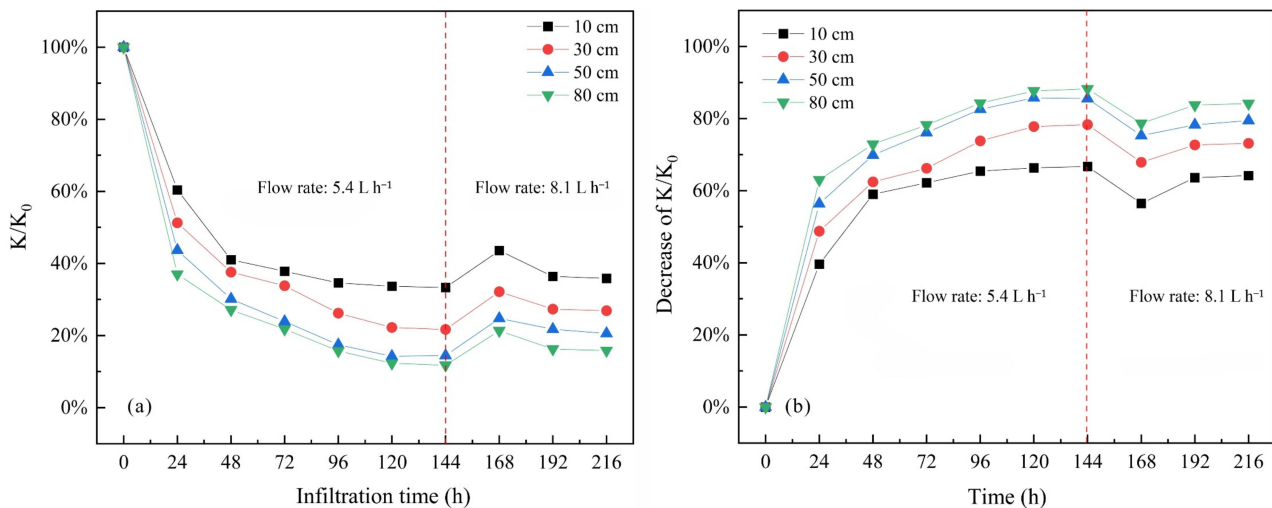


**Figure 2.** The variation of relative hydraulic conductivity (a), and decreased degree of relative hydraulic conductivity (b).  $K$  denotes the measured hydraulic conductivity ( $m d^{-1}$ );  $K_0$  denotes the initial hydraulic conductivity ( $m d^{-1}$ ).

After increasing the inflow rate, the RHC recovered to a certain degree, then decreased, and finally reached a new steady state (Figure 2). The lower the infiltration distance, the better the recovery of RHC. The average of RHC in the simulated RBF system (15.8–35.9%) at 216 h was higher than it at 144 h (11.8–33.3%). It indicated that the flushing could recover the permeability of the medium in RBF system to a certain extent, while the clogging was still inevitable due to the RHC values at the new steady state being higher than those at 144 h without increasing inflow velocity.

### 3.2. Variation of Water Quality Parameters

The box plot of the concentration of target water quality parameters is shown in Figure S1. The variation of each parameter in different infiltration depths during the RBF process was also shown in the following sections.

#### 3.2.1. Turbidity

The curve of the turbidity ratio ( $T/T_0$ ) kept decreasing from 0 to 120 h, and the range of decline was 59.4–96.9% after 96 h (Table S2, Figure 3). Similar to the variation of RHC mentioned in Section 3.1, the decline of turbidity ratio increased with the increase of the infiltration distance, resulting in the average values of turbidity ratio being in an order of 80 cm (79.6–96.9%) > 50 cm (77.2–94.9%) > 30 cm (72.5–85.0%) > 10 cm (59.4–78.6%) (Table S2). Meanwhile, the turbidity ratio continuously increased after 96 h in the infiltration path of 10 and 30 cm, while it kept almost constant in the after 120 h infiltration path of 50–80 cm. It might represent a discrepancy in purification capacity for removing suspended particles at different infiltration distances.

With increasing the inflow rate, the turbidity ratio also increased from 144 h to 168 h, then declined in 168–192 h, and reached a new steady state at 216 h (Figure 3). The increase of turbidity ratio during 144–168 h was in an order of 10 cm (11.2%) > 30 cm (9.5%)

> 50 cm (7.9%) > 80 cm (6.2%). Meanwhile, the average value of turbidity ratio in the simulated RBF system (14.1%) at 216 h was higher than it at 144 h (12.2%).

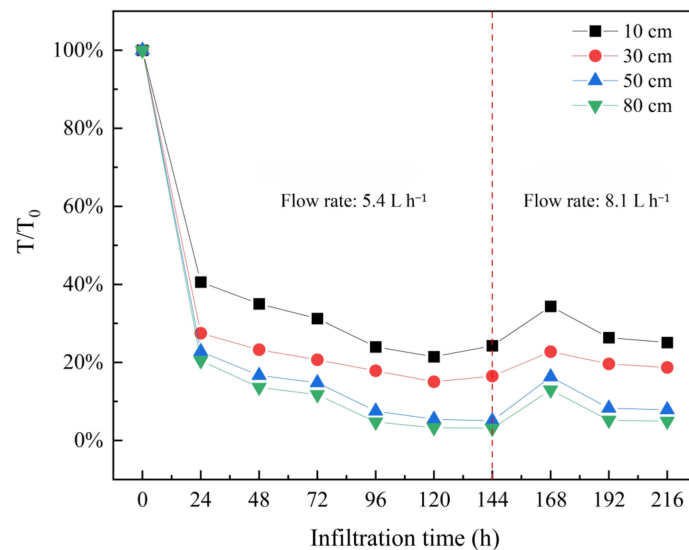


**Figure 3.** The variation of relative turbidity.  $T$  denotes the measured turbidity (NTU) from samples;  $T_0$  denotes the initial turbidity in the raw water (NTU).

### 3.2.2. $\text{NH}_4^+$ and COD

The concentration variation of  $\text{NH}_4^+$  and COD was similar (Figure 4). In general, the relative concentration of  $\text{NH}_4^+$  and COD kept decreasing, which were 60.6–89.1% and 28.3–78.1%, respectively, in the time period of 0–120 h (Table S1). Meanwhile, the relative concentration of  $\text{NH}_4^+$  and COD almost remained unchanged in 120–144 h, which demonstrated that they might have reached a steady state in 120–144 h during RBF. After increasing the inflow velocity, the relative concentration of COD increased by 4.0–10.5%; whereas, the relative concentration of  $\text{NH}_4^+$  slightly decreased by 1.7–2.0% from 144 h to 168 h, and then reached the new steady state at 216 h (Figure 4). The decline of  $\text{NH}_4^+$  and COD also increased with the infiltration distance, which, reflecting the infiltration distance (or residence time), might affect the water quality improvement capacity of the RBF system.

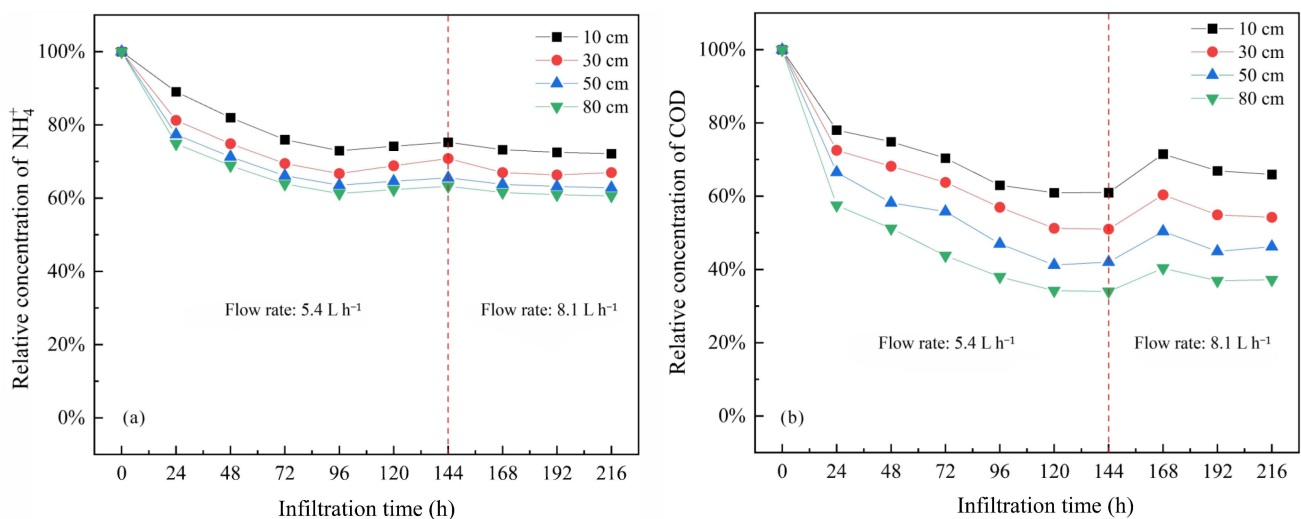


**Figure 4.** The variation of the relative concentration of  $\text{NH}_4^+$  (a) and COD (b), respectively.

### 3.2.3. Mn and Fe

The variations in the relative concentrations of Mn(IV) and  $\text{Mn}^{2+}$  were 36.1–83.2% and 29.3–82.2%, respectively, during the experiment, which was not as remarkable as other parameters (Figure 5). It decreased in 0–120 h, and then rose in 120–144 h. After increasing flow rate ( $8.1 \text{ L h}^{-1}$ ), the relative concentration of Mn(IV) and  $\text{Mn}^{2+}$  decreased and almost reached the new steady states from 144 h to 216 h, which were 36.1–62.0% and 29.3–57.0% respectively. Interestingly, the discrepancy in the relative concentration of Mn(IV) and  $\text{Mn}^{2+}$  between 10 cm and 30 cm was not remarkable. A similar phenomenon was also found between 50 cm and 80 cm. It indicated that the removal of Mn was significant with the infiltration distance of 30–50 cm. Moreover, there was a significant gap between 10–30 cm and 50–80 cm. The relative concentrations of Mn(IV) and  $\text{Mn}^{2+}$  at 50–80 cm were obviously lower than those in 10–30 cm. It demonstrated that the removal mechanism might be different from the physical sorption (e.g., variation of turbidity), and further leading to the different clogging mechanism.

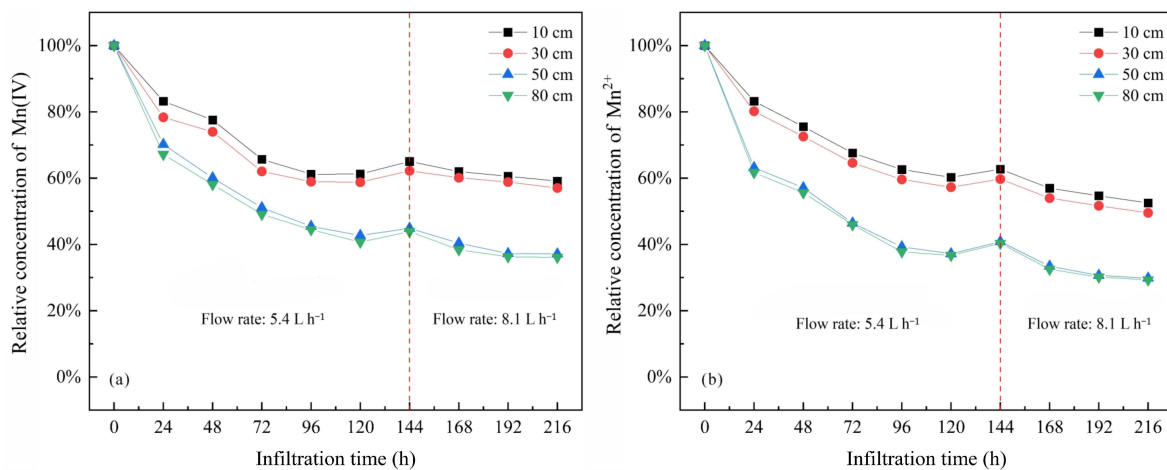


**Figure 5.** The variation in the relative concentrations of Mn(IV) (a) and  $\text{Mn}^{2+}$  (b), respectively.

The variation in the relative concentrations of  $\text{Fe}^{2+}$ ,  $\text{Fe}^{3+}$ , and total Fe were 35.2–81.4%, 45.2–86.4%, and 43.1–85.3%, respectively, which were not as significant as other parameters (Figure 6). Similar to the variation of Mn, the discrepancy in the relative concentration of  $\text{Fe}^{2+}$ ,  $\text{Fe}^{3+}$ , and total Fe between 10 cm and 30 cm was not remarkable. Meanwhile, there was an obvious gap in relative concentration between 50 cm and 80 cm. The relative concentration of  $\text{Fe}^{2+}$ ,  $\text{Fe}^{3+}$ , and total Fe at 80 cm were obviously lower than those at 50 cm. It demonstrated that the removal mechanism might be different from the physical sorption (e.g., variation of turbidity), and further promoted the clogging at infiltration distance of 50–80 cm.

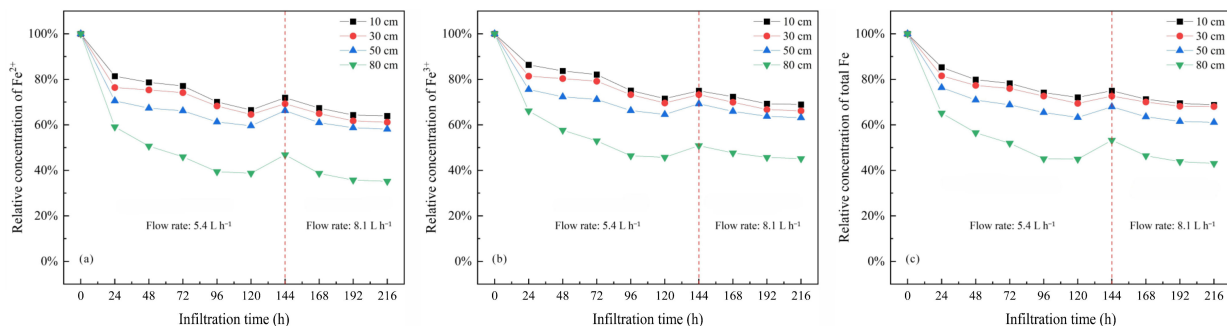


**Figure 6.** The variation of relative concentration of  $\text{Fe}^{2+}$  (a),  $\text{Fe}^{3+}$  (b), and total Fe (c).

### 3.3. PCA and Network Analysis

PCA was applied to identify the clogging processes of RBF in the experiment. It was implemented for 37 water samples. As shown in Table S4, two principal components (PC1 and PC2) with eigenvalues exceeding 1 were extracted, describing 90.76% of the total variance. The PC1 exhibited strong loadings of total Fe (0.961),  $\text{Fe}^{3+}$  (0.957), Mn(IV) (0.955),  $\text{Mn}^{2+}$  (0.952),  $\text{Fe}^{2+}$  (0.95), turbidity (0.883),  $\text{NH}_4^+$  (0.862), and infiltration distance ( $-0.795$ ), which explained 80.2% of the total variance. It contained most of the physicochemical variables, representing that the clogging processes should be mixed effects, including physical and chemical clogging. The PC2 exhibited strong loadings of COD (0.972) and time ( $-0.748$ ), which explained 10.6% of the total variance.

To further estimate the impacts of physical and chemical clogging on RBF, the network analysis was conducted to identify clogging patterns of the target water quality parameters in different infiltration distances. The positive correlations edge accounted for 64.4%, which was greater than the negative correlations edge (35.6%). As shown in Figure 7, the diaphaneity of edges showed the correlation strength between each parameter. Specifically, within the infiltration distance of 10 cm, there was a significant negative correlation between turbidity and permeability ( $r = -0.95$ ,  $p < 0.01$ ) (Figure 7a). The edge between those two parameters was also more distinct than other parameters. It illustrated that the decrease of suspended particle contents should be the principal reason for clogging at 10 cm. For 30 cm, the edge between turbidity and permeability became weaker; meanwhile, the negative correlation relationships between permeability and  $\text{NH}_4^+$  ( $r = -0.53$ ,  $p < 0.05$ ), permeability and Mn(IV) ( $r = -0.47$ ,  $p < 0.05$ ), and permeability and  $\text{Mn}^{2+}$  ( $r = -0.4$ ,  $p < 0.05$ ) became more distinct than those in 10 cm (Figure 7b). It indicated that  $\text{NH}_4^+$ , Mn(IV), and  $\text{Mn}^{2+}$  might affect the permeability due to the chemical clogging during RBF at 30 cm. For 50 cm, the edges between Mn(IV) and permeability ( $r = -0.76$ ,  $p < 0.01$ ) and  $\text{Mn}^{2+}$  and permeability ( $r = -0.75$ ,  $p < 0.01$ ) became more obvious than those in 10 cm and 30 cm (Figure 7c). In addition, the significant negative correlations between Mn(IV) and  $\text{Mn}^{2+}$  ( $r = -0.71$ ,  $p < 0.01$ ) were more significant than in other infiltration distances, meaning that there should be a reduction process between Mn(IV) and  $\text{Mn}^{2+}$  at 30–50 cm. For 80 cm, the correlations between Mn(IV) and permeability ( $r = -0.27$ ,  $p < 0.05$ ) and  $\text{Mn}^{2+}$  and permeability ( $r = -0.30$ ,  $p < 0.05$ ) were not as significant as it in 30 cm and 50 cm. However, the edges between  $\text{Fe}^{2+}$ ,  $\text{Fe}^{3+}$ , total Fe, and permeability were more remarkable than those in 10–50 cm (Figure 7d). The correlation coefficients between  $\text{Fe}^{2+}$ ,  $\text{Fe}^{3+}$ , total Fe, and permeability were  $-0.77$  ( $p < 0.01$ ),  $-0.79$  ( $p < 0.01$ ), and  $-0.60$  ( $p < 0.05$ ), respectively. Meanwhile, the negative correlations between  $\text{Fe}^{2+}$  and  $\text{Fe}^{3+}$  ( $r = -0.99$ ,  $p < 0.01$ ),  $\text{Fe}^{2+}$ , and total Fe ( $r = 0.83$ ,  $p < 0.01$ ) were more significant than those in other infiltration distances, showing that there should be reduction processes between  $\text{Fe}^{2+}$ ,  $\text{Fe}^{3+}$ , and total Fe at 50–80 cm.

In general, with the increase of infiltration distance, the edge between turbidity and permeability became weaker. The correlation between Mn and permeability was significant in 30–50 cm, additionally, the correlation between Fe and permeability was significant in 50–80 cm. It demonstrated that the clogging mechanisms might be different in these infiltration distances due to the variation correlation between target parameters.

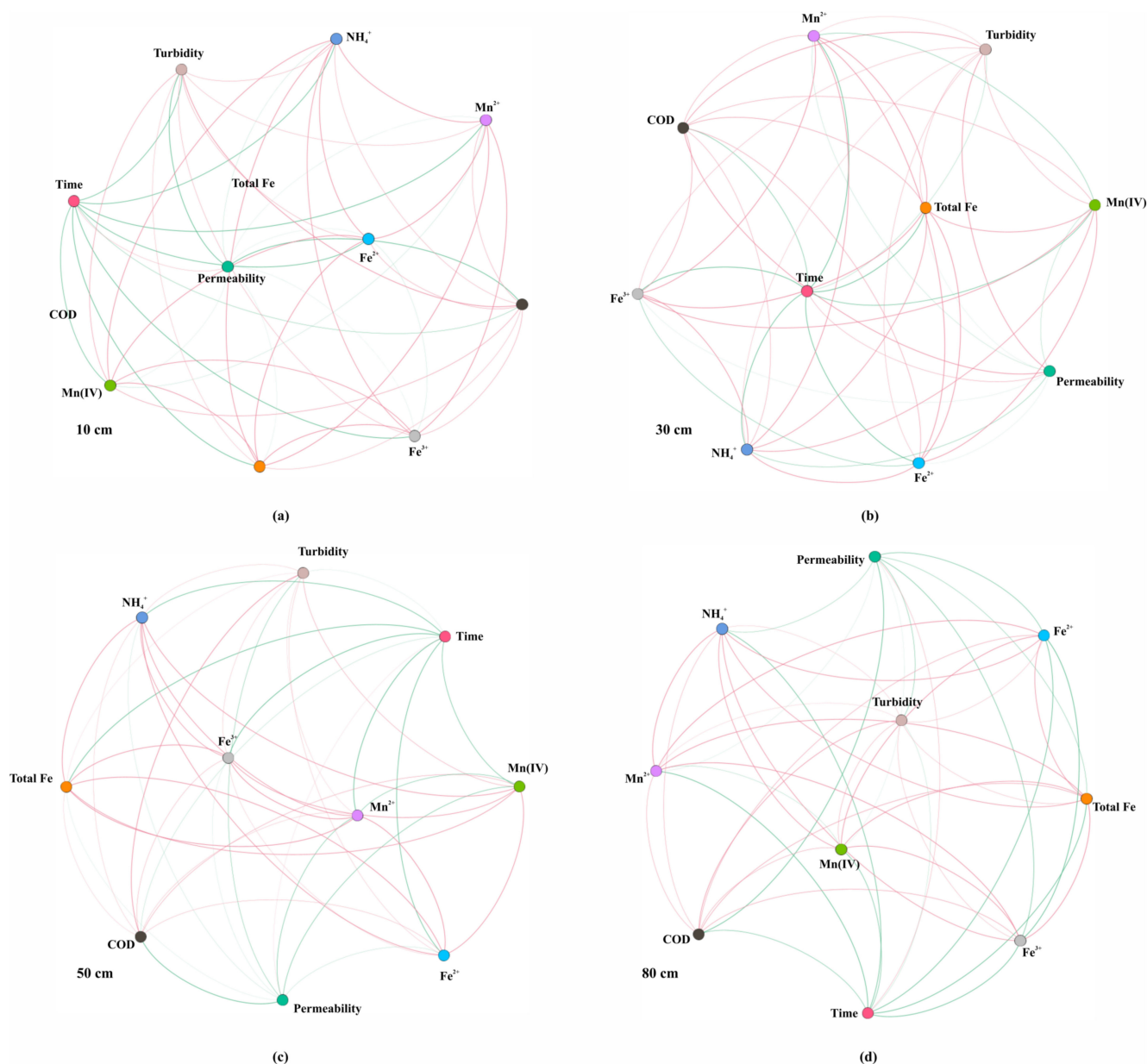


**Figure 7.** Network analysis of the water quality parameters in 10 cm (a), 30 cm (b), 50 cm (c), and 80 cm (d), respectively. Node colors indicate different water quality parameters. Each shown connection represents a Spearman correlation coefficient. Green lines denote a negative correlation, and red lines denote a positive correlation. The higher the absolute value of the correlation coefficient for each two parameters have, the more distinct the lines are.

## 4. Discussion

### 4.1. Clogging Mechanisms

During the progress of the experiment set-up, biocidal treatment with HgCl<sub>2</sub> was implemented during the progress of the experiment set-up to avoid biomass development. Thus, the clogging mechanisms in this study mainly refer to physical and chemical clogging.

#### 4.1.1. Physical Clogging

As shown in the variation of relative hydraulic conductivity (Figure 2) and network analysis (Figure 7), the removal of turbidity has represented the suspended particle removal by RBF, as well as the suspended materials deposition [21,29,36]. The significant negative correlation between permeability and removal of the turbidity ( $r = -0.812$ ,  $p < 0.01$ ) also

demonstrated the occurrence of physical clogging issue in the whole infiltration pathway (Table S3). As in the previous studies, the concentration of the suspended particles is one of the major factors affecting the physical clogging [47–49], which is consistent with the findings of the simulated experiment in this study. In the view of residence time and infiltration distance, the physical clogging in the experiment dominated in 0–96 h and 144–168 h at 0–10 cm, which equals 0–12.5% of the infiltration pathway. During the river water infiltrating into the aquifer, inorganic, and organic suspended particles can be trapped in the riverbed pore channels and/or aquifer mediums [26], inducing physical clogging issues. The intense seepage process in the riverbed and/or aquifer always occurs in the front areas of the infiltration pathway. Noting that, the increase of flow rate can recover the turbidity ratio and relative hydraulic conductivity to a certain degree, indicating that the sediment flushing can relieve the clogging issues to some degree, and finally reach a new steady state between clogging and river water infiltration. Thus, the clogging issue is inevitable during RBF although conducting some mitigation measures [3,27,39].

#### 4.1.2. Chemical Clogging

According to the experiment results, during the continuous variation of water quality parameters, chemical clogging has also occurred in the meantime. The increase of the aqueous concentrations of COD,  $\text{NH}_4^+$ ,  $\text{Mn}^{2+}$ , and  $\text{Fe}^{2+}$  suggests that the chemical clogging dominated in 120–144 h and 192–216 h at 30–80 cm, which equals 37.5–100% of the infiltration pathway (Table S4). The significant negative correlations between permeability and concentration of target water quality parameters also illustrated the occurrence of chemical clogging in the 30–80 cm (Table S3). Due to the precipitation of soluble components, ion exchange sorption, and redox reaction, the precipitates and adsorbates can accumulate in pores, therefore leading to chemical clogging in the riverbed sediments, aquifer media, and nearby the groundwater withdrawal wells [50–52]. Besides, the existed significant gaps in Mn and Fe concentration demonstrated that Mn(IV) reduction and Fe(III) reduction zones were 30–50 cm and 50–80 cm, respectively (Figure 7). It is also consistent with the intense areas of chemical clogging occurrence, which are caused by redox reaction, on permeability at 30–80 cm.

When the inflow rate increases to 1.5 times ( $8.1 \text{ L h}^{-1}$ ) the original inflow rate ( $5.1 \text{ L h}^{-1}$ ) after 144 h, the relative concentrations of  $\text{NH}_4^+$ , Mn(IV),  $\text{Mn}^{2+}$ , total Fe,  $\text{Fe}^{2+}$ , and  $\text{Fe}^{3+}$  decreased in different degrees (Figures 4–6). With the increase in inflow rate, a larger quantity of oxygenated water infiltrated into the simulated system than before, therefore changing the redox conditions, which can further decrease  $\text{NH}_4^+$ ,  $\text{Mn}^{2+}$ , total Fe, and  $\text{Fe}^{2+}$  by oxidation reactions. Meanwhile, the increased flow rate also strengthens the dilution effect on every water quality parameter during the infiltration process. As previous studies reported, chemical clogging often takes certain periods to develop [3,53,54]. In other words, the increased rate of oxidation reactions does not match the dilution effect in this study. This is why those water quality parameters mentioned above are all still decreasing after increasing the inflow rate.

Additionally, there should be a mixed area existing at 10–30 cm infiltration pathway with the co-impacts of both physical and chemical clogging. However, the contribution of each clogging mechanism in this area cannot be clearly divided in this study. Thus, 12.5–37.5% of the infiltration pathway can be regarded as a transition zone for dominating clogging mechanism transforming from physical to chemical (Table S5).

#### 4.2. Impact Factors for Clogging in the RBF System

The porosity of the sediment and initial flow rate are the principal factors governing the clogging depth [23]. The PCA result demonstrated that duration of time and redox condition are also impact factors for clogging development (Table S4). For physical clogging, the concentration of suspended particle materials, mean size of riverbed sediments, and aquifer media are the major impact factors [52,55]. Meanwhile, due to the deposition of suspended particle materials, physical clogging induced by cake build-up on the surface

of the riverbed and aquifer can reduce riverbed and aquifer permeability [56,57]. Usually, physical clogging is reversible and dominant in the top layer, which is consistent with the observation of a significant decrease and recovery of RHC at 0–12.5% of the infiltration pathway (0–10 cm in this study) with two inflow rates during the experiment. For chemical clogging, the precipitation of soluble constituents (e.g.,  $\text{FeCO}_3$ , iron hydroxides), redox reaction, and other hydrochemical processes are major impact factors [48,58]. When oxygenated water infiltrates into the aquifers, the redox conditions changed, motivating precipitation of Fe and Mn hydroxides. The precipitates accumulation in pores can result in chemical clogging dominating in the middle and bottom layers. Different from physical clogging, the chemical clogging induced by chemical processes is typically irreversible and takes a certain time for development [36,56]. It is consistent with the findings of COD, Mn, and Fe concentration variation at 37.5–100% of the infiltration pathway (30–80 cm in this study).

## 5. Conclusions

With the continuous operation of RBF, the clogging process can affect groundwater withdrawal by decreasing the hydraulic conductivity and pores in riverbed and aquifer media, which is inevitable. Based on laboratory column experiments, the physical and chemical clogging mechanisms in the RBF site with a long-distance infiltration pathway to the Lalin River were studied. The decline of relative hydraulic conductivity was generally increased with the infiltration pathway, which ranged from 39.6–88.2% for the infiltration distance of 10–80 cm, respectively. After biocidal treatment, the major clogging mechanisms during the experiments are the following two types: (i) physical clogging caused by suspended particle materials deposition; and (ii) chemical clogging caused by precipitation of soluble components (e.g.,  $\text{FeCO}_3$ ), ion exchange sorption, and redox reaction (e.g., Mn and Fe). Among them, the physical clogging occurs in the whole infiltration pathway, which was remarkable at 0–12.5% of the infiltration pathway; the chemical clogging dominated in 37.5–100% of the infiltration pathway. Meanwhile, there was a transition zone for physical clogging transforming to chemical clogging at 12.5–37.5% of the infiltration pathway. Moreover, the porosity of the sediment, initial flow rate, and duration of time are the principal factors for governing the clogging depth. For physical clogging, which is usually reversible and dominated in the top layer of the infiltration channel, the concentration of suspended particle materials, mean size of riverbed sediments, and aquifer media are the major impact factors. For chemical clogging, which is usually irreversible and occurs in the middle and bottom layers of the infiltration channel, the precipitation of soluble constituents, redox reaction, and other hydrochemical processes are major impact factors. The impacts of biofilm formation and biomass accumulation on the permeability of RBF sites have been proved by other studies [33]. Whereas, biological clogging was not discussed in the study due to the biocidal treatment. Thus, the impacts and mechanisms of biological clogging on the waterworks near Lalin River, which has used RBF technology, need further study in the future.

**Supplementary Materials:** The following supporting information can be downloaded at: <https://www.mdpi.com/article/10.3390/su14159330/s1>, Table S1: Statistical summary of the experimental data of water samples; Table S2: Statistical summary of removal rate of water quality parameters during RBF simulation experiment; Table S3: Correlation matrix of the water quality parameters; Table S4: Principal component loadings of the water quality parameters; Table S5: Statistical summary of removal rate of water quality parameters during RBF simulation experiment; Figure S1: The box plot of concentration of target water quality parameters.

**Author Contributions:** Conceptualization, B.H.; methodology, L.L.; software, H.C.; validation, B.H., P.L. and R.C.; investigation, B.H. and L.L.; resources, B.H.; data curation, B.H. and Y.L.; writing—original draft preparation, B.H.; writing—review and editing, B.H. and G.L.; visualization, B.H. and R.C.; supervision, G.L. and Y.T.; project administration, G.L. and Y.T.; funding acquisition, B.H., G.L. and Y.T. All authors have read and agreed to the published version of the manuscript.

**Funding:** This research was funded by the National Natural Science Foundation of China (41877355), National Key R&D Program of China (2018YFE0204100), Postdoctoral Research Foundation of China (2020M680698), the Open Project Program of Engineering Research Center of Groundwater Pollution Control and Remediation, Ministry of Education of China (GW202102), and Beijing Advanced Innovation Program for Land Surface Science.

**Institutional Review Board Statement:** Not applicable.

**Informed Consent Statement:** Not applicable.

**Data Availability Statement:** Not applicable.

**Conflicts of Interest:** The authors declare no conflict of interest.

## References

1. Ray, C.; Grischek, T.; Schubert, J.; Wang, J.Z.; Speth, T.F. A perspective of riverbank filtration. *J. Am. Water Work. Assoc.* **2002**, *94*, 149–160. [\[CrossRef\]](#)
2. Gupta, V.; Johnson, W.P.; Shafieian, P.; Ryu, H.; Alum, A.; Abbaszadegan, M.; Hubbs, S.; Rauch-Williams, T. Riverbank filtration: Comparison of pilot scale transport with theory. *Environ. Sci. Technol.* **2009**, *43*, 669–676. [\[CrossRef\]](#) [\[PubMed\]](#)
3. Hu, B.; Teng, Y.; Zhai, Y.; Zuo, R.; Li, J.; Chen, H. Riverbank filtration in China: A review and perspective. *J. Hydrol.* **2016**, *541*, 914–927. [\[CrossRef\]](#)
4. Singh, P.; Kumar, P.; Mehrotra, I.; Grischek, T. Impact of riverbank filtration on treatment of polluted river water. *J. Environ. Manag.* **2010**, *91*, 1055–1062. [\[CrossRef\]](#)
5. Covatti, G.; Grischek, T. Sources and behavior of ammonium during riverbank filtration. *Water Res.* **2021**, *191*, 116788. [\[CrossRef\]](#)
6. Nagy-Kovács, Z.; Davidesz, J.; Czihat-Mártonné, K.; Till, G.; Fleit, E.; Grischek, T. Water quality changes during riverbank filtration in Budapest, Hungary. *Water* **2019**, *11*, 302. [\[CrossRef\]](#)
7. Nartowska, E.; Kozłowski, T.; Gawdzik, J. Assessment of the influence of copper and zinc on the microstructural parameters and hydraulic conductivity of bentonites on the basis of SEM tests. *Heliyon* **2019**, *5*, e02142. [\[CrossRef\]](#)
8. Bach, M.; Letzel, M.; Kaul, U.; Forstner, S.; Metzner, G.; Klasmeier, J.; Reichenberger, S.; Frede, H. Measurement and modeling of bentazone in the river Main (Germany) originating from point and non-point sources. *Water Res.* **2010**, *44*, 3725–3733. [\[CrossRef\]](#)
9. Abdelrady, A.; Sharma, S.; Sefelnasr, A.; Abogbal, A.; Kennedy, M. Investigating the impact of temperature and organic matter on the removal of selected organic micropollutants during bank filtration: A batch study. *J. Environ. Chem. Eng.* **2019**, *7*, 102904. [\[CrossRef\]](#)
10. Sprenger, C.; Lorenzen, G.; Hülshoff, I.; Grützmacher, G.; Ronghang, M.; Pekdeger, A. Vulnerability of bank filtration systems to climate change. *Sci. Total Environ.* **2011**, *409*, 655–663. [\[CrossRef\]](#)
11. Guellouz, L.; Askri, B.; Jaffré, J.; Bouhlila, R. Estimation of the soil hydraulic properties from field data by solving an inverse problem. *Sci. Rep.* **2020**, *10*, 9359. [\[CrossRef\]](#)
12. Ghodeif, K.; Grischek, T.; Bartak, R.; Wahaab, R.; Herlitzius, J. Potential of river bank filtration (RBF) in Egypt. *Environ. Earth Sci.* **2016**, *75*, 671. [\[CrossRef\]](#)
13. Farnsworth, C.E.; Hering, J.G. Inorganic geochemistry and redox dynamics in bank filtration settings. *Environ. Sci. Technol.* **2011**, *45*, 5079–5087. [\[CrossRef\]](#)
14. Dillon, P.; Miller, M.; Fallowfield, H.; Hutson, J. The potential of riverbank filtration for drinking water supplies in relation to microcystin removal in brackish aquifers. *J. Hydrol.* **2002**, *266*, 209–221. [\[CrossRef\]](#)
15. Massmann, G.; Sültenfuß, J.; Dünnebier, U.; Knappe, A.; Taute, T.; Pekdeger, A. Investigation of groundwater residence times during bank filtration in Berlin: A multi-tracer approach. *Hydrol. Process.* **2008**, *22*, 788–801. [\[CrossRef\]](#)
16. Dash, R.R.; Bhanu Prakash, E.; Kumar, P.; Mehrotra, I.; Sandhu, C.; Grischek, T. River bank filtration in Haridwar, India: Removal of turbidity, organics and bacteria. *Hydrogeol. J.* **2010**, *18*, 973–983. [\[CrossRef\]](#)
17. Hiscock, K.M.; Grischek, T. Attenuation of groundwater pollution by bank filtration. *J. Hydrol.* **2002**, *266*, 139–144. [\[CrossRef\]](#)
18. Wang, W.-S.; Oswald, S.E.; Gräff, T.; Lensing, H.-J.; Liu, T.; Strasser, D.; Munz, M. Impact of river reconstruction on groundwater flow during bank filtration assessed by transient three-dimensional modelling of flow and heat transport. *Hydrogeol. J.* **2020**, *28*, 723–743. [\[CrossRef\]](#)
19. Tufenkji, N.; Ryan, J.N.; Elimelech, M. Peer reviewed: The promise of bank filtration. *Environ. Sci. Technol.* **2002**, *36*, 422A–428A. [\[CrossRef\]](#)
20. Ulrich, C.; Hubbard, S.S.; Florsheim, J.; Rosenberry, D.; Borglin, S.; Trotta, M.; Seymour, D. Riverbed clogging associated with a California riverbank filtration system: An assessment of mechanisms and monitoring approaches. *J. Hydrol.* **2015**, *529*, 1740–1753. [\[CrossRef\]](#)
21. Poojitha, S.; Hari Prasad, K.; Ojha, C. Effect of Clogging on Riverbank Filtration: An Experimental Analysis Using Ganges Riverbed Sediment. *J. Hazard. Toxic Radioact.* **2022**, *26*, 04021065. [\[CrossRef\]](#)
22. Martins, M.; Lunardi, S.; de Andrade Puhl, V.; Pizzolatti, B.S.; Soares, M. Enzymatic analysis in bank filtration sites as a tool for assessing biological clogging—A column study. *J. Water Process Engl.* **2021**, *44*, 102375. [\[CrossRef\]](#)

23. Huston, D.L.; Fox, J.F. Clogging of fine sediment within gravel substrates: Dimensional analysis and macroanalysis of experiments in hydraulic flumes. *J. Hydraul. Eng.* **2015**, *141*, 04015015. [[CrossRef](#)]
24. Cunningham, A.; Anderson, C.; Bouwer, H. Effects of sediment-laden flow on channel bed clogging. *J. Irrig. Drain Eng.* **1987**, *113*, 106–118. [[CrossRef](#)]
25. Schubert, J. Experience with riverbed clogging along the Rhine River. In *Riverbank Filtration Hydrology*; Hubbs, S.A., Ed.; Springer: Dordrecht, The Netherlands, 2006; pp. 221–242.
26. Gutiérrez, J.P.; van Halem, D.; Uijtewaal, W.S.; Del Risco, E.; Rietveld, L.C. Natural recovery of infiltration capacity in simulated bank filtration of highly turbid waters. *Water Res.* **2018**, *147*, 299–310. [[CrossRef](#)]
27. Cui, G.; Su, X.; Liu, Y.; Zheng, S. Effect of riverbed sediment flushing and clogging on river-water infiltration rate: A case study in the Second Songhua River, Northeast China. *Hydrogeol. J.* **2021**, *29*, 551–565. [[CrossRef](#)]
28. Sakellariou-Makrantonaki, M.; Angelaki, A.; Evangelides, C.; Bota, V.; Tsianou, E.; Floros, N. Experimental determination of hydraulic conductivity at unsaturated soil column. *Proc. Procedia Eng.* **2016**, *162*, 83–90. [[CrossRef](#)]
29. Goldschneider, A.A.; Haralampides, K.A.; MacQuarrie, K.T. River sediment and flow characteristics near a bank filtration water supply: Implications for riverbed clogging. *J. Hydrol.* **2007**, *344*, 55–69. [[CrossRef](#)]
30. Miszkowska, A.; Lenart, S.; Koda, E. Changes of permeability of nonwoven geotextiles due to clogging and cyclic water flow in laboratory conditions. *Water* **2017**, *9*, 660. [[CrossRef](#)]
31. Sahu, R.L.; Dash, R.R.; Pradhan, P.K.; Das, P. Effect of hydrogeological factors on removal of turbidity during river bank filtration: Laboratory and field studies. *Groundw. Sustain. Dev.* **2019**, *9*, 100229. [[CrossRef](#)]
32. Angelaki, A.; Dionysidis, A.; Sihag, P.; Golia, E.E. Assessment of Contamination Management Caused by Copper and Zinc Cations Leaching and Their Impact on the Hydraulic Properties of a Sandy and a Loamy Clay Soil. *Land* **2022**, *11*, 290. [[CrossRef](#)]
33. Hubbs, S.A. Changes in riverbed hydraulic conductivity and specific capacity at Louisville. In *Riverbank Filtration Hydrology*; Hubbs, S.A., Ed.; Springer: Dordrecht, The Netherlands, 2006; pp. 199–220.
34. Engesgaard, P.; Seifert, D.; Herrera, P. Bioclogging in porous media: Tracer studies. In *Riverbank Filtration Hydrology*; Hubbs, S.A., Ed.; Springer: Dordrecht, The Netherlands, 2006; pp. 93–118.
35. Westrich, B.; Förstner, U. *Sediment Dynamics and Pollutant Mobility in Rivers—An Interdisciplinary Approach*; Springer: Berlin, Germany, 2007.
36. Pholkern, K.; Srisuk, K.; Grischek, T.; Soares, M.; Schäfer, S.; Archwichai, L.; Saraphirom, P.; Pavelic, P.; Wirojanagud, W. Riverbed clogging experiments at potential river bank filtration sites along the Ping River, Chiang Mai, Thailand. *Environ. Earth Sci.* **2015**, *73*, 7699–7709. [[CrossRef](#)]
37. Ray, C. Conclusions and Recommendations of the NATO Advanced Research Workshop: Contaminant Biogeochemistry and Pathogen Removal Efficiency. In *Riverbank Filtration: Understanding Contaminant Biogeochemistry and Pathogen Removal*; Springer: Berlin/Heidelberg, Germany, 2002; pp. 247–250.
38. Ranjan, P.; Prem, M. Schmutzdecke—a filtration layer of slow sand filter. *Int. J. Curr. Microbiol. Appl. Sci.* **2018**, *7*, 637–645. [[CrossRef](#)]
39. Grischek, T.; Bartak, R. Riverbed clogging and sustainability of riverbank filtration. *Water* **2016**, *8*, 604. [[CrossRef](#)]
40. Thakur, A.; Ojha, C.; Singh, V.; Gurjar, B.R.; Sandhu, C. Removal of pathogens by river bank filtration at Haridwar, India. *Hydrol. Process.* **2013**, *27*, 1535–1542. [[CrossRef](#)]
41. Hu, B.; Teng, Y.; Li, T.; Zhai, Y.; Zuo, R.; Chen, H. Clogging characteristics of riverbank filtration wells and its alleviating approaches. *Geol. Sci. Technol. Inform.* **2016**, *35*, 178–183. (In Chinese)
42. Zhang, Y.; Hubbard, S.; Finsterle, S. Factors governing sustainable groundwater pumping near a river. *Groundwater* **2011**, *49*, 432–444. [[CrossRef](#)]
43. Wang, L.; Ye, X.; Du, X. Suitability evaluation of river bank filtration along the Second Songhua River, China. *Water* **2016**, *8*, 176. [[CrossRef](#)]
44. Song, W.; Liu, X.; Zheng, T.; Yang, J. A review of recharge and clogging in sandstone aquifer. *Geothermics* **2020**, *87*, 101857. [[CrossRef](#)]
45. Zhai, Y.; Xia, X.; Yang, G.; Lu, H.; Ma, G.; Wang, G.; Teng, Y.; Yuan, W.; Shrestha, S. Trend, seasonality and relationships of aquatic environmental quality indicators and implications: An experience from Songhua River, NE China. *Ecol. Eng.* **2020**, *145*, 105706. [[CrossRef](#)]
46. Li, J.; Chen, H.; Teng, Y.; Dong, Q. Contamination characteristics and source apportionment of soil heavy metals in Lalin River basin. *Trans. Chin. Soc. Agric. Eng.* **2016**, *32*, 226–233. (In Chinese)
47. Blaschke, A.P.; Steiner, K.H.; Schmalfluss, R.; Gutknecht, D.; Sengschmitt, D. Clogging processes in hyporheic interstices of an impounded river, the Danube at Vienna, Austria. *Int. Rev. Hydrobiol.* **2003**, *88*, 397–413. [[CrossRef](#)]
48. Bouwer, H. Artificial recharge of groundwater: Hydrogeology and engineering. *Hydrogeol. J.* **2002**, *10*, 121–142. [[CrossRef](#)]
49. Pavelic, P.; Dillon, P.; Mucha, M.; Nakai, T.; Barry, K.; Bestland, E. Laboratory assessment of factors affecting soil clogging of soil aquifer treatment systems. *Water Res.* **2011**, *45*, 3153–3163. [[CrossRef](#)]
50. Du, X.; Wang, Z.; Ye, X. Potential clogging and dissolution effects during artificial recharge of groundwater using potable water. *Water Resour. Manag.* **2013**, *27*, 3573–3583. [[CrossRef](#)]
51. Schubert, J. Hydraulic aspects of riverbank filtration—Field studies. *J. Hydrol.* **2002**, *266*, 145–161. [[CrossRef](#)]

52. Caldwell, T.G. Presentation of data for factors significant to yield from several riverbank filtration systems in the US and Europe. In *Riverbank Filtration Hydrology*; Hubbs, S.A., Ed.; Springer: Dordrecht, The Netherlands, 2006; pp. 299–344.
53. Oberleitner, D.; Schulz, W.; Bergmann, A.; Achten, C. Impact of seasonality, redox conditions, travel distances and initial concentrations on micropollutant removal during riverbank filtration at four sites. *Chemosphere* **2020**, *250*, 126255. [[CrossRef](#)]
54. Ascott, M.; Lapworth, D.; Gooddy, D.; Sage, R.; Karapanos, I. Impacts of extreme flooding on riverbank filtration water quality. *Sci. Total Environ.* **2016**, *554*, 89–101. [[CrossRef](#)]
55. Stuyfzand, P.J.; Juhász-Holterman, M.H.; Lange, W.J.D. Riverbank filtration in the Netherlands: Well fields, clogging and geochemical reactions. In *Riverbank Filtration Hydrology*; Hubbs, S.A., Ed.; Springer: Dordrecht, The Netherlands, 2006; pp. 119–153.
56. Seiler, K.-P.; Gat, J. Mechanisms and processes of recharge. In *Groundwater Recharge from Run-Off, Infiltration and Percolation*; Springer: Dordrecht, The Netherlands, 2007; pp. 31–68.
57. Du, X.; Fang, Y.; Wang, Z.; Hou, J.; Ye, X. The prediction methods for potential suspended solids clogging types during managed aquifer recharge. *Water* **2014**, *6*, 961–975. [[CrossRef](#)]
58. Zhang, H.; Ye, X.; Du, X. Laws and mechanism of the Fe (III) clogging of porous media in managed aquifer recharge. *Water* **2021**, *13*, 284. [[CrossRef](#)]